Science Advances

AAAS

advances.sciencemag.org/cgi/content/full/3/4/e1602697/DC1

Supplementary Materials for

Maximizing the performance of photothermal actuators by combining smart materials with supplementary advantages

Tongyu Wang, David Torres, Félix E. Fernández, Chuan Wang, Nelson Sepúlveda

Published 21 April 2017, *Sci. Adv.* **3**, e1602697 (2017)
DOI: 10.1126/sciadv.1602697

The PDF file includes:

Other Supplementary Material for this manuscript includes the following:
(available at advances.sciencemag.org/cgi/content/full/3/4/e1602697/DC1)

- movie S1 (.wmv format). Wavelength-selective actuation of the VO_2 actuator.
- movie S2 (.wmv format). Wavelength-selective actuation of the VO_2/uSWNT actuator.
- movie S3 (.wmv format). Wavelength-selective actuation of the VO_2/mSWNT actuator.
- movie S4 (.wmv format). Wavelength-selective actuation of the VO_2/sSWNT actuator.

note S1. Photothermal response measurement.

Figure S3 illustrates the setup for photothermal response measurement. Two semiconducting laser diodes with wavelengths of 660 nm and 985 nm were used for light illumination. It is noted that the shape and size of laser spots for each laser are different, which could result in uneven intensity distribution. In order to solve this problem, laser beams were coupled into single mode optical fibres (P2-630A-PCSMA-1 and P2-980A-PCSMA-1 from Thorlabs), which reshape the beam profiles and output standard single mode laser beams. Newport laser driver (Model 505B) controlled by Labview program was used to vary the driving current to the laser, and consequently its power output.

The sample was placed on top of a Petier heater mounted on a two dimensional translation stage which was used to align test samples with the laser beam. The temperature was controlled by Labview program through Thorlab temperature controller TED4015. Shown in fig. S3, CCD camera NO. 1 assists the alignment of laser sand samples, while CCD camera NO. 2, with the help of a high magnification lens (Mitutoyo, f=200 mm), monitors the actuators' motion from side view. Between samples and driving laser, a lens was used to manipulate the diameter of the laser spot on test samples to be 500 μm (measured by a beam profiler Thorlab BP209-VIS) for both wavelengths. Videos of CCD camera NO.2 containing displacement information were processed by Tracker software to track the movement of cantilevers' tip during photothermal actuation and extract displacement data. For the time response measurement, a high speed camera (Nikon 1 with 1,200 fps) was used to for capturing displacement.

During the photothermal actuation, the laser spot was first aligned with actuators to have maximum displacement at a pre-heat temperature of 45 ^{o}C, then the laser was turned off. After the temperature of actuators was reset to 40 ^{o}C, the measurement was carried out by varying the power of laser illumination. After one photothermal measurement for one wavelength, the fiber of new wavelength was installed on the fiber adapter that stay unchanged through this procedure. In this way, the positions of two laser of different wavelengths were maintained the same. In time response measurement, an external trigger signal (square wave with 25 ms pulse width and 50% duty cycle) was connected to laser current driver to generate shot laser pulses.

note S2. Wavelength selectivity study for various SWNT film thickness.

The band structure of SWNT with selective chirality endows the material with intriguing wavelength selective optical properties (shown in Fig. 2A). However, the optical absorption is not the only parameter that influences absorption in a thin film. According to Beer-Lambert's law, the transmittance across a film decreases with the film's thickness. For a SWNT film with specific chirality distribution, the absorption of all wavelengths increases as the film gets thicker. Eventually, the absorption of all wavelengths will saturate (close to 100%), and the wavelength selective spectrum will become indistinctive. Here, we studied the relation between SWNT film thickness and its absorption spectrum, which allowed for the design of a film thickness suitable for our devices.

As an example, the absorption spectrum of semiconducting SWNT films for different thickness is shown in fig. S7. For 100 nm thick semiconducting SWNT film, the spectrum shows an absorption peak at ~1000 nm, while for 200 nm thick film, the absorption peak becomes almost unnoticeable. For 500 nm thick film, most of the light is absorbed by the film regardless of the wavelength, causing a near flat spectrum and no wavelength selectivity. Given this relation between wavelength selectivity and film thickness, we used 100 nm thick SWNT film to fabricate the wavelength selective micro-actuators. It should also be noticed that thinner films could give better wavelength selective spectrum shape, but then the total absorbed power will also decrease; thus increasing the laser intensity requirement for inducing the phase transition of the VO_2 thin film.

note S3. Movie information.

Movies that are included in the supplementary materials show the wavelength selective actuation (presented in Fig. 3) of four different types of actuators: VO_2 (movie S1.wmv), VO_2/uSWNT (movie S2.mp4), VO_2/mSWNT (movie S3.mp4), and VO_2/sSWNT (movie S4.mp4). The first part of the movies show displacement under 660 nm light pulses of 30 mW, and the second part of the movies show displacement under 985 nm pulses of 30 mW. The deflections observed in the movies follow the same measured responses plotted in Figs. 2C–F and 3.

note S4. Photothermal actuation model of VO2/SWNT actuators.

A model based on finite element method (FEM) was created in COMSOL with physics of "Heat Transfer" and "Solid Mechanics". The phase transition of VO_2 was modelled by a temperature dependent thermal expansion coefficient $\alpha(T)$ (*37*)

$$\alpha(T) = \frac{6\times10^{-6}}{1+e^{-0.2(T-226.15)}} - 3\times10^{-8}(T-273.15) + 6.9\times10^{-6} \quad \text{(S1)}$$

which is obtained from a curve fit to the experimental measurement. A heat influx on the surface of actuators acts as the light illumination, while the anchor was set to be 40°C same as experiments. The air convection was applied to the model with convection cooling coefficient h_{air} which is a function of dimensions of the device and calculated by the software. The parameters used in the model are summarized in table S1.

First, a "Stationary" study was performed to calculate the stabilized temperature distribution on the actuators with laser irradiation. The light intensity distribution on the actuators is complicated as a result of beams' Gaussian profile and unknown exact location of the laser spot. Hence, we assume that heat influx intensity is uniform in the model, and fitted the simulated deflection with the measured deflection, matching the power used in the experiments. The results are shown Fig. 5 with temperature distribution on the actuator's surface, along the cantilever's length, and for different devices.

In order to study the dynamic performance of this type of actuators, we studied the photothermal and mechanical processes. For obtaining the time response associated with the photothermal mechanism, the following heat transfer equation (S2) is used

$$\rho C_p \frac{\partial T}{\partial t} = \nabla\cdot(k\nabla T) + Q \quad \text{(S2)}$$

where ρ is density of VO_2 and SWNT film, C_p is the specific heat, T is temperature, t is time, k is thermal conductivity, and Q contains all heat source. The convective cooling of air and light illumination were introduced by following equations (S3) and (S4)

$$-\boldsymbol{n}\cdot\left(-k\nabla T\right)=h_{air}\left(T_{ext}-T\right) \tag{S3}$$

$$-\boldsymbol{n}\cdot\left(-k\nabla T\right)=I_{light} \tag{S4}$$

where $\boldsymbol{n}$ is normal vector of the surface, h_{air} is air convection cooling coefficient that is a function of structure geometry, T_{ext} is external temperature, and I_{light} is the laser intensity on the actuators. Figure S5 shows the time dependent temperature curve of VO_2/uSWNT, VO_2/mSWNT , and VO_2/sSWNT actuators, in which the step input light illumination (40 mW) was applied at 5 ms. The response time that enables 90% of full actuation, is calculated to be 2.65, 3.0, and 2.82 ms, respectively.

For obtaining the time response associated to the structure's mechanical behavior, we studied structural resonance frequencies. Here, the "Eigenfrequency" study in COMSOL was used to characterize VO_2/uSWNT actuators' mechanical resonance frequencies. It is important to notice that additional stress and strain inside the structure caused by temperature increase during actuation could change its resonance frequencies. Therefore, the initial values including temperature, displacement, and stress for "Eigenfrequency" study were imported from a "Stationary" study under same light illumination (40 mW). The first resonance frequency mode ω_n calculated is ~6 kHz, and for a second order underdamping system ($0 < \zeta < 1$) the rise time τ of an unit step input can be approximated to equation (S5) (*38*)

$$t_r \cong \frac{1-0.4167\zeta+2.917\zeta^2}{\omega_n} \tag{S5}$$

indicating a fast response time in the range of 0.16 ms $< \tau <$ 0.6 ms. Clearly, the thermal process dominates the response time for the photothermal actuation of these devices, and a faster response is obtained by improving the photothermal process, which in this work is achieved by the higher absorption of SWNT films (see Fig. 4).

note S5. Effects of different thermal conductivities and heat capacities between SWNT films.

Photothermal actuation process is analyzed in two steps. First, the light is absorbed by the SWNT films and converted to thermal energy. This process is mainly determined by the optical properties of SWNT films, and it is the process that allows for the wavelength-selective added multifunctionality of the reported devices. The second step involves the distribution of thermal energy over the actuator structure. Thermal conductivity and heat capacity of the structural materials (i.e. SWNT films, VO_2 layers, and SiO_2) play a role in the photothermal process.

Since both processes occur simultaneously, it is very difficult to analyze them individually by using experimental studies. Thus, two finite element method simulations were performed: one using different values for heat capacity (while keeping the thermal conductivity constant), and another using different values for thermal conductivity (while keeping the heat capacity constant).

Heat capacity variations: The heat capacity used in the manuscript for all the SWNT films is 550 J/(kg·K), which is the value for uSWNT films (*14*). The heat capacity values for the other films (i.e. mSWNT and sSWNT) is not available in the literature. However, in order to study the effects of possible changes in the time response due to different heat capacities between SWNT films, we proceeded to run simulations for three different heat capacity values: 350, 550, and 750 J/(kg·K). Figure S8 shows the temperature increase for the three cases as a function of time for the same input. It can be noticed that the curves are almost overlapping, with the largest difference in response time being only 0.09 ms, which is found between the 350 and 750 J/(kg·K) curves. This means that doubling the heat capacity only produces a change in the time response of about 3%. Therefore, variations in the heat capacity of the SWNT films have little effect on the response time.

Heat capacity relates to the amount of energy that is required to increase the temperature of a given mass of the material --it should be noted that heat capacity does not play a role in the final equilibrium temperature. With constant incident illumination power (constant

absorbed heat), SWNT films with lower heat capacity require less energy to increase temperature, and therefore reach equilibrium temperature faster. This is why the response time increases with heat capacity. However, the role of heat capacity in the time response in our devices is mostly dominated by the VO_2 and SiO_2 layers –the difference in heat capacities of the different SWNT has very little effect on determining the time response of the device. Assuming the average temperature increase of the actuators is ΔT, the absorbed optical energy power is h_l, and the average power of heat loss power through conduction at the anchor and convection of the surfaces is h_{cc}, the total energy required to complete the heating process can be expressed as following equation

$$\mathrm{E} = \left(\rho_{SWNT} C_{SWNT} d_{SWNT} + \rho_{VO_2} C_{VO_2} d_{VO_2} + \rho_{SiO_2} C_{SiO_2} d_{SiO_2} \right) S \Delta T = \tau \left(h_l - h_{cc} \right) \qquad \text{(S6)}$$

where ρ is the density, C is heat capacity, S is surface area, d is the thickness of different layers, and τ is the response time. The SWNT films are only 100 nm thick, and have a density of 1500 kg/m^3. The VO_2 and SiO_2 layers, on the other hand, are 50 nm and 1000 nm thick; have densities of 4670 and 2200 kg/m^3; and their heat capacities are 700 and 730 J/(kg·K), respectively. This means that VO_2 and SiO_2 layers play a much more important role in determining the energy required to reach equilibrium temperature; and explains the small change in time response (only 3%) for an increase in heat capacity from 350 to 750 J/(kg·K).

Thermal conductivity variations: We ran simulations using the new thermal conductivity values: 121, 192, and 242 W/(m·K) for the mSWNT, sSWNT, and uSWNT, respectively; while keeping all the other simulation parameters equal (the heat capacity used for the simulations is 550 J/(kg·K)). Figure S9 shows the response times obtained from the simulation, and the corresponding response curves are shown in fig. S5. It can be noticed that the response time decreases with thermal conductivity. The response times are 3.0, 2.82, and 2.65 ms, for the mSWNT, sSWNT, and uSWNT devices, respectively. Higher thermal conductivity can help distribute the heat faster across the actuator. As a result, the temperature settling time is smaller, meaning lower thermal response time.

note S6. Effects of SWNT film thickness in wavelength selectivity.

The optical absorption of SWNT thin films are determined by two factors, thickness (*d*) and attenuation coefficient (σ). The absorption rate can be expressed as $Ab = 1 - Tr - Sc$, where *Ab* is absorption rate, *Tr* is transmittance, and *Sc* is scattering. Assuming *Ab* + *Tr* >> *Sc*, then the equation can be simplified as $Ab \approx 1 - Tr$. Based on Beer-Lambert law, the absorption rate that is dependent on wavelengths in the case of SWNT films can be expressed as a function of thickness and attenuation coefficient in the following way

$$Ab(\lambda, d) = 1 - e^{-\sigma(\lambda)d} \tag{S7}$$

The wavelength selectivity of a film can be quantitatively characterized as the difference of absorption for two wavelengths, as shown below

$$\Delta Ab = Ab(\lambda_1, d) - Ab(\lambda_2, d) = e^{-\sigma(\lambda_2)d} - e^{-\sigma(\lambda_1)d} \tag{S8}$$

Then the partial derivative of ΔAb with respect to the variable *d* can be expressed as

$$\frac{\partial \Delta Ab}{\partial d} = \sigma_1 e^{-\sigma_1 d} - \sigma_2 e^{-\sigma_2 d} \tag{S9}$$

where $0 \le d \le \infty$; and $\sigma(\lambda_1)$ and $\sigma(\lambda_2)$ have been re-defines as σ_1 and σ_2, respectively. Assuming $\sigma_1 > \sigma_2$, the plot of Eqns. (S8) and (S9) are qualitatively shown in fig. S10.

When $\frac{\partial \Delta Ab}{\partial d} = 0$, ΔAb reaches the highest point. Solving Eqn. (S9) = 0 for "*d*" results in the thickness for highest absorption difference for two wavelengths, which is

$$d = \frac{\ln\left(\frac{\sigma_1}{\sigma_2}\right)}{\sigma_1 - \sigma_2} \tag{S10}$$

The attenuation coefficient of SWNT films can be estimated from the measured

absorbance (see Fig. S7) by using $\sigma = \frac{A \ln 10}{d_{100}}$, where d_{100} = 00 nm (thickness of the SWNT films in the experiments), and A is the measured absorbance. Using the estimated attenuation coefficient for a thickness of 100 nm, we can then estimate the optimal thickness for mSWNT and sSWNT films to be d_m = 119, and d_s = 91 nm, respectively. For experiments, we chose a thickness of 100 nm, which is approximately a midpoint.

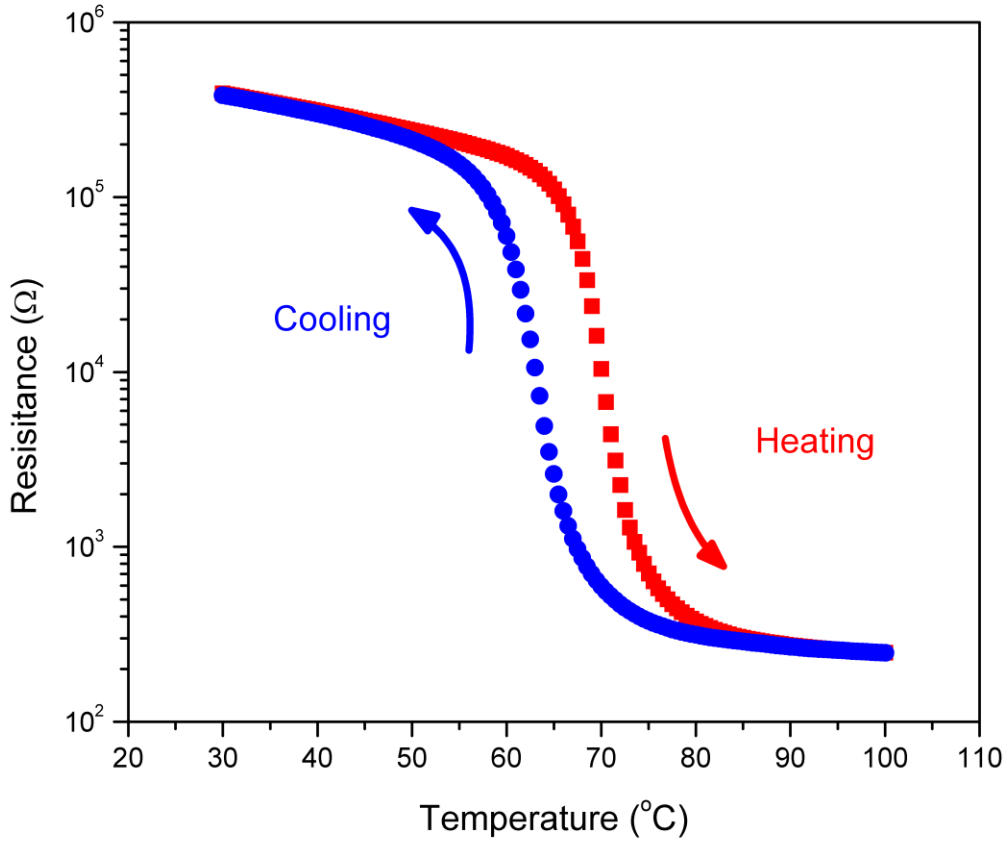

fig. S1. Resistance of VO_2 as a function of temperature. The figure shows a ~3 order drop when temperature is cycled across the phase transition from 30°C to 100°C.

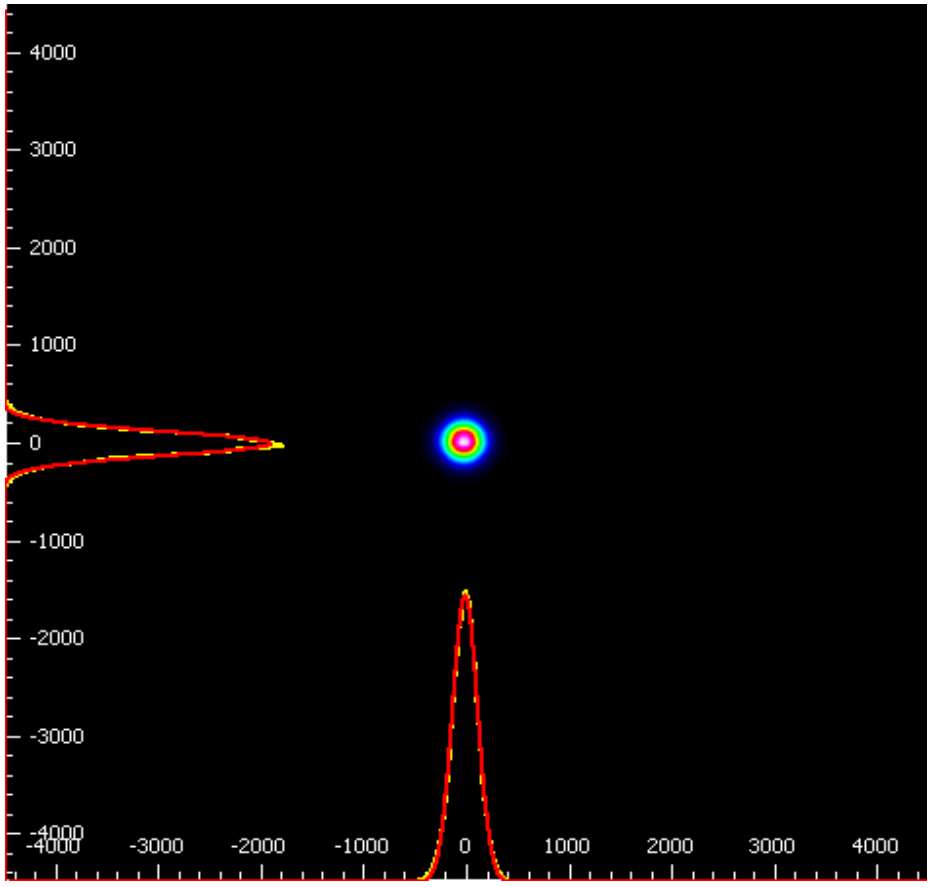

fig. S2. Beam profiles for the lasers on the tested actuators. The beam profiles were measured by Thorlabs Dual Scanning Slit Beam Profiler BP209-VIS. The maximum intensity in the circular profile decayed by 13.5% at a diameter of 500 μm in both x and y directions. Yellow curves represent real measured data, while the red curves are Gaussian fits.

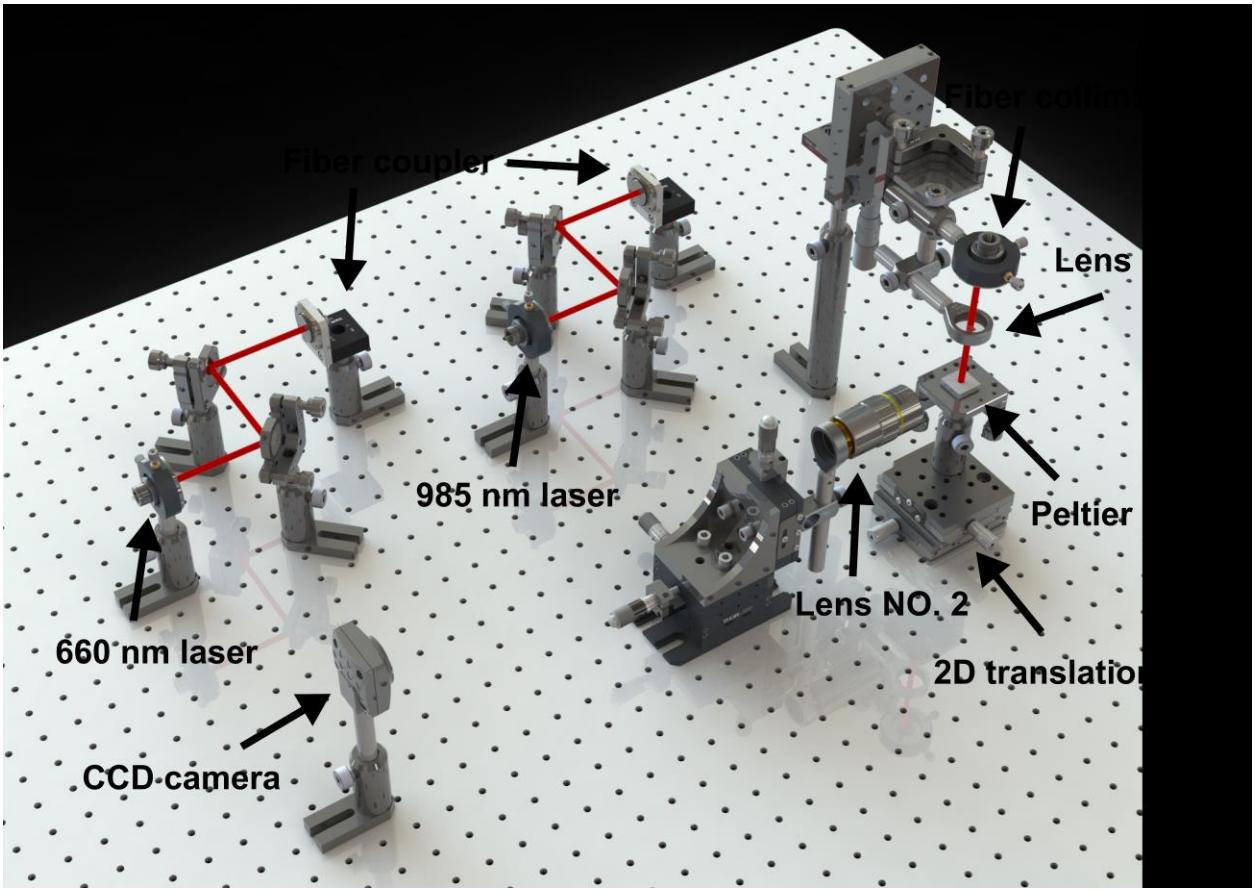

fig. S3. Schematic of the setup used for photothermal and time response measurements. Two lasers are coupled into two single mode optical fibers, which are not shown in the diagram for clarity. Light coming out of the fiber collimator is focused by lens NO. 1 on the samples. The Peltier heater was used to control the temperature of the sample, either for pre-heating or conductive actuation experiments. CCD camera was used to record deflections of actuators with help of high amplification lens NO. 2.

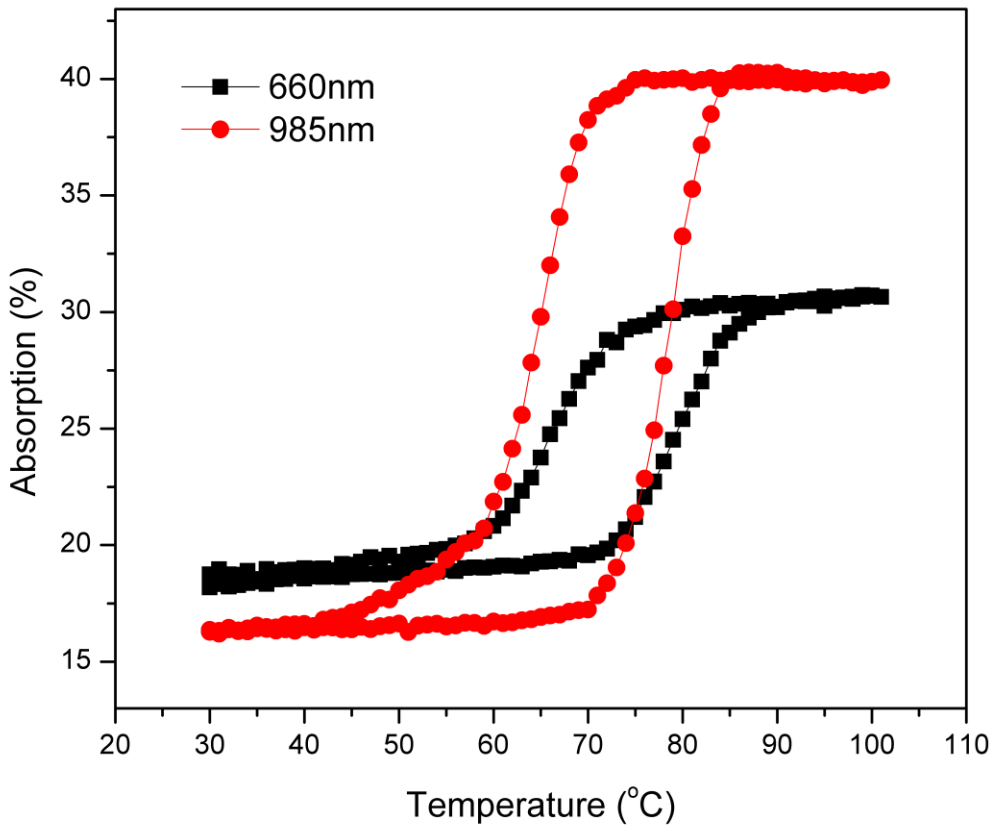

fig. S4. Light absorption of the VO_2 thin film. The VO_2 film was deposited on SiO_2 substrate, and the absorption was measured as a function temperature for wavelengths of 660 nm and 985 nm. Absorption (*Ab*) was calculated by measuring transmittance (*T*r), reflectance (*R*), and then using $Ab = (1 - Tr - R) \times 100\%$.

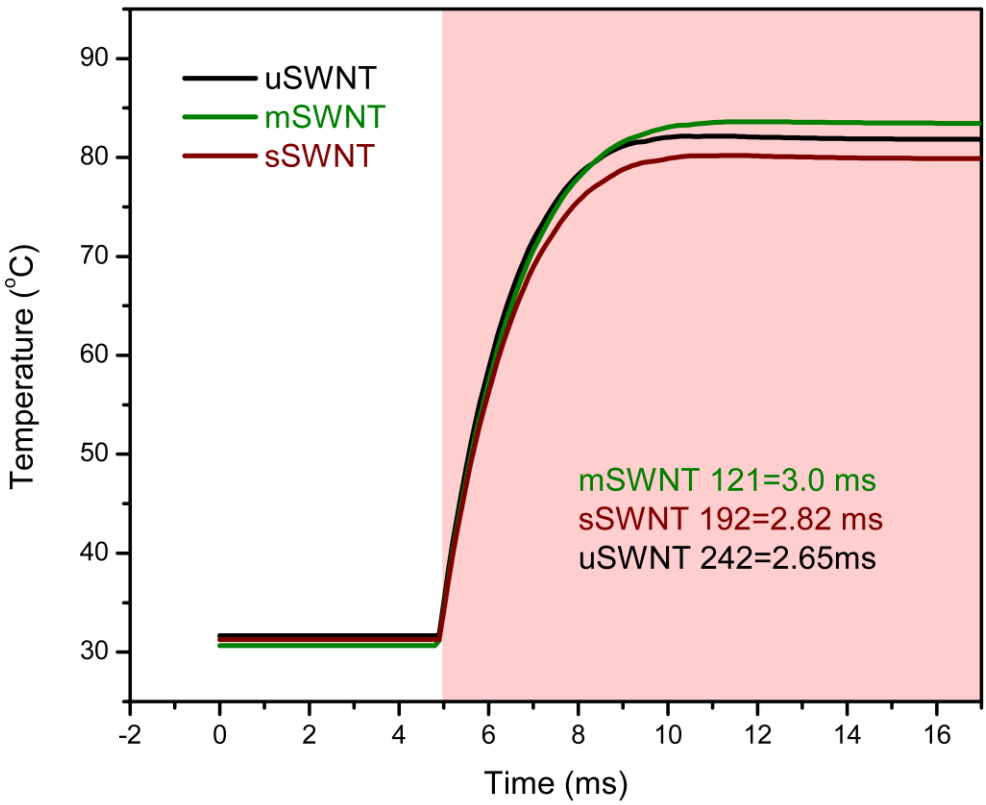

fig. S5. Simulated temperature change as a function of time. The step input of light illumination is applied on actuators at 5 ms.

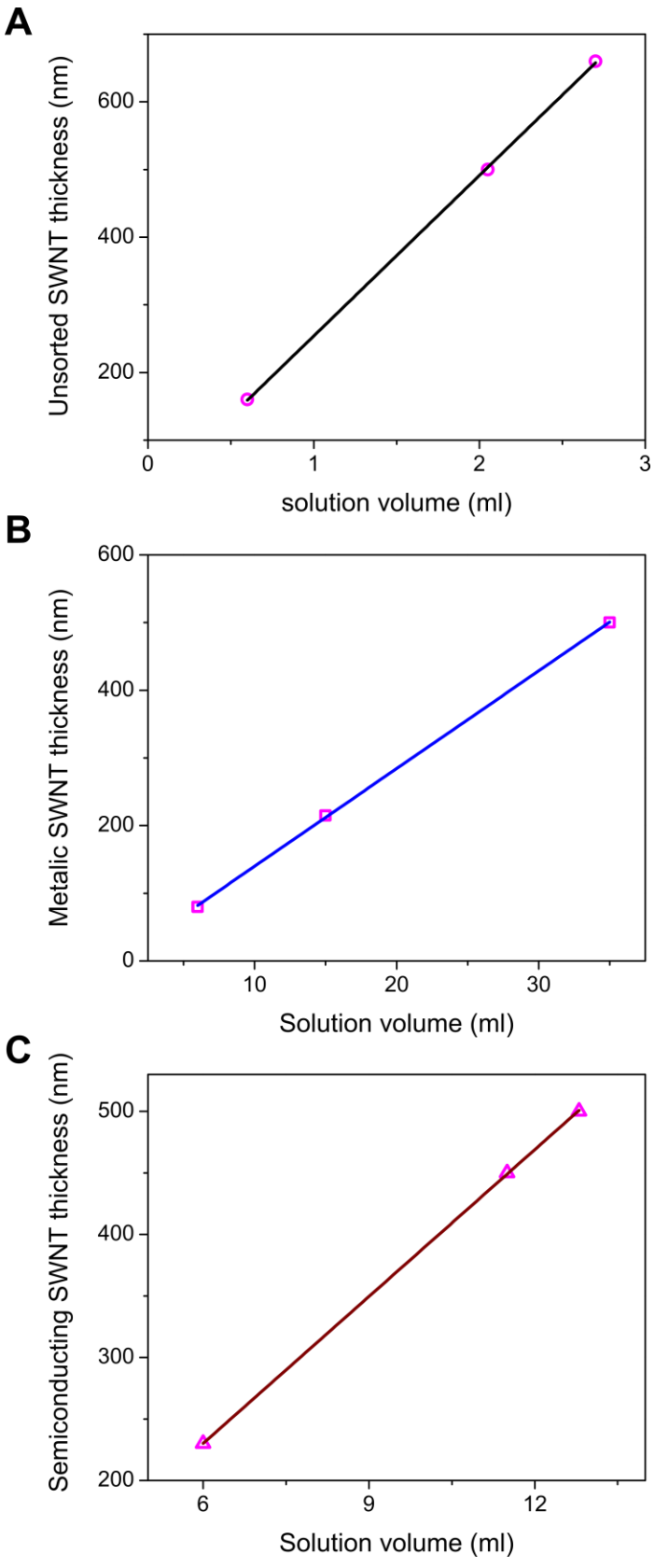
A
Unsorted SWNT thickness (nm)
600
400
200
0
1
2
3
solution volume (ml)
B
Metalic SWNT thickness (nm)
600
400
200
0
10
20
30
Solution volume (ml)
C
Semiconducting SWNT thickness (nm)
500
400
300
200
6
9
12
Solution volume (ml)

fig. S6. The SWNT film thickness versus the volume of SWNT solution used for vacuum filtration. The concentration of uSWNT (**A**), mSWNT (**B**), and sSWNT (**C**) solution is ~0.5 mg/ml, 0.01 mg/ml, and 0.01 mg/ml, respectively. The thickness of the SWNT thin film can be readily controlled by adjusting the amount of SWNT solution.

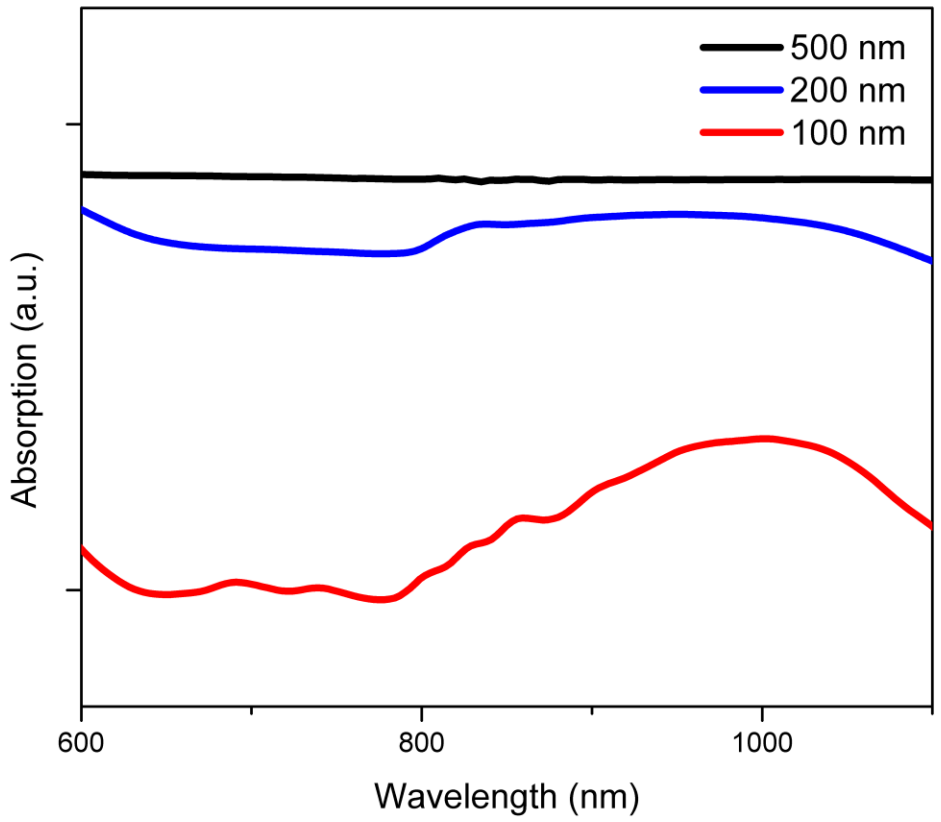

fig. S7. Absorption spectra of sSWNT films for different thicknesses. The wavelength selectivity of semiconducting SWNT thin film degrades as the thickness increases.

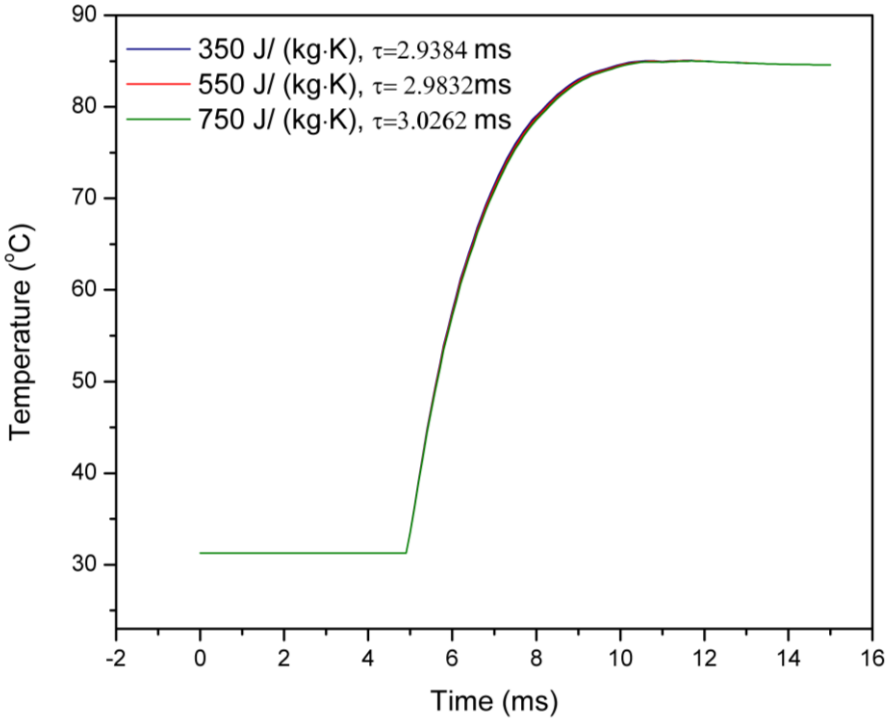

fig. S8. Photothermal response of SWNT films with different heat capacities. The difference in response time for the SWNT actuators is not significantly influenced by the heat capacity of the SWNT film. An increase in heat capacity from 350 to 750 J/(kg·K) changes the time response by only 3%.

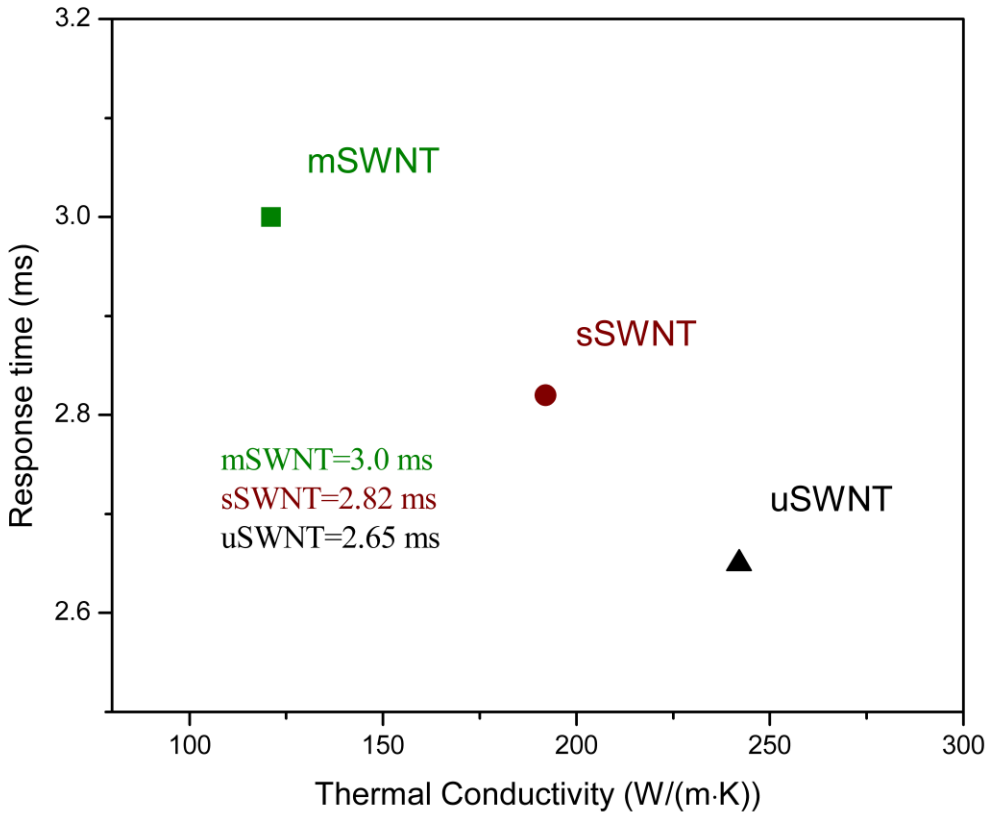

fig. S9. Response time versus SWNT film thermal conductivity. The response time for the actuators increases with decreasing thermal conductivity.

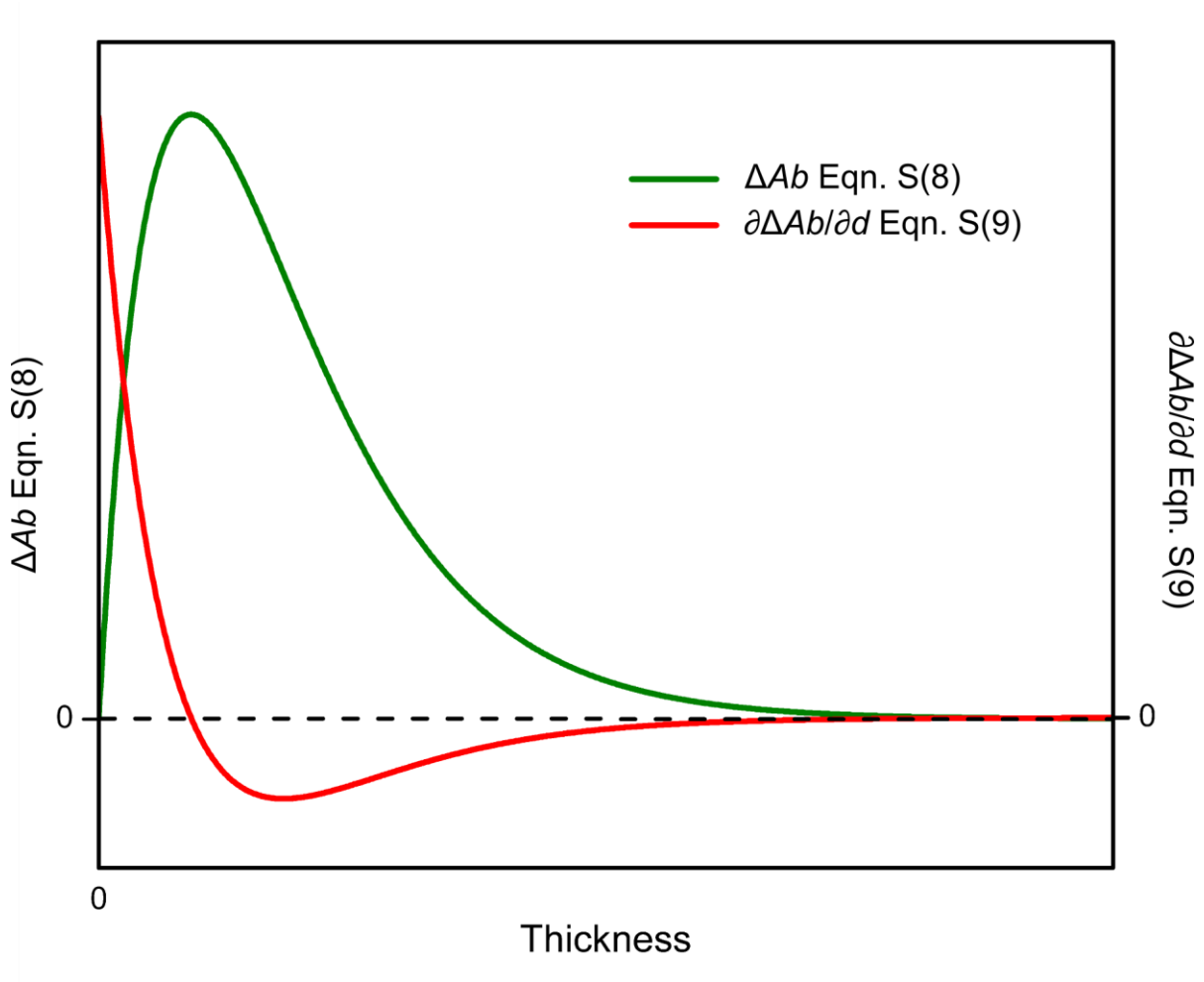

fig. S10. Wavelength selectivity as a function of thickness. The largest difference in absorption for two wavelengths occurs when the thickness of mSWNT or sSWNT films is 119 and 91 nm, respectively.

table S1. Material properties used in the FEM model. The thermal expansion coefficient of VO_2, $\alpha(T)$, is a function of temperature T, and its expression is stated in note S4.

	VO_2 (*38*)	**uSWNT (*14, 39*)**		
Density (kg/m^3)	4670	1500		
Young's modulus (GPa)	140	1.5		
Thermal conductivity ($W \cdot m^{-1} \cdot K^{-1}$)	5	uSWNT	mSWNT	sSWNT
		242	121	191
Thermal expansion coefficient (K^{-1})	$\alpha(T)$	3×10^{-6}		
Specific heat ($J \cdot kg^{-1} \cdot K^{-1}$)	700	550		

movie S1. Wavelength-selective actuation of the VO_2 actuator.

movie S2. Wavelength-selective actuation of the VO_2/uSWNT actuator.

movie S3. Wavelength-selective actuation of the VO_2/mSWNT actuator.

movie S4. Wavelength-selective actuation of the VO_2/sSWNT actuator.